Large deviations of the current for driven periodic diffusions

Pelerine Tsobgni Nyawo[1,*] and Hugo Touchette[1,2,†]
[1]*Institute of Theoretical Physics, Department of Physics, University of Stellenbosch, Stellenbosch 7600, South Africa*
[2]*National Institute for Theoretical Physics (NITheP), Stellenbosch 7600, South Africa*
(Received 8 June 2016; published 1 September 2016)

We study the large deviations of the time-integrated current for a driven diffusion on the circle, often used as a model of nonequilibrium systems. We obtain the large deviation functions describing the current fluctuations using a Fourier-Bloch decomposition of the so-called tilted generator, and we also construct from this decomposition the effective (biased, auxiliary, or driven) Markov process describing the diffusion as current fluctuations are observed in time. This effective process provides a clear physical explanation of the various fluctuation regimes observed. It is used here to obtain an upper bound on the current large deviation function, which we compare to a recently derived entropic bound, and to study the low-noise limit of large deviations.

DOI: 10.1103/PhysRevE.94.032101

I. INTRODUCTION

In this paper, we study the driven diffusion on the circle defined by the following stochastic differential equation (SDE):

$$d\theta_t = [\gamma - V'(\theta_t)]dt + \sigma\, dW_t, \tag{1}$$

where $\theta_t \in [0,2\pi)$, $V(\theta)$ is a periodic potential taken to be

$$V(\theta) = V_0 \cos\theta, \tag{2}$$

$\gamma \in \mathbb{R}$ is a constant driving frequency, and W_t is Brownian motion multiplied by the noise intensity $\sigma \geqslant 0$. This SDE represents one of the simplest nonequilibrium system violating detailed balance for $\gamma \neq 0$, and has played as such an important role in the development and illustration of recent results about nonequilibrium response [1–4], entropy production [5–7], and large deviations in the long-time [8–12] or low-noise [13–15] regime. It is also used as a model of Josephson junctions subjected to thermal noise [16–18], Brownian ratchets [19], and manipulated Brownian particles [20–22], among other systems (see [1]), and it is thus an ideal experimental testbed for the physics of nonequilibrium systems.

In this paper, we use large deviation theory to study the fluctuations of a natural observable of the driven diffusion, its mean velocity, defined formally as

$$J_T = \frac{1}{T}\int_0^T \dot{\theta}_t\, dt. \tag{3}$$

Previous works have looked at the large deviations of this quantity [10,11], which also represents a time-integrated fluctuating current for the diffusion, as well as the large deviations of the entropy production [5–7], which is linearly related to J_T. Our goal here is to complete these studies by investigating the large deviation functions characterizing the fluctuations of J_T in all noise regimes and by constructing the *auxiliary process*, also known as the *biased* or *driven process*, describing the diffusion conditionally upon observing a current fluctuation $J_T = j$ far from the mean current $\langle J_T \rangle$. This process is physically important as it describes, by means of a modified stochastic process, how fluctuations of the current or any time-integrated observable in general are created in time [23–28].

This effective description of fluctuations was illustrated recently in the context of interacting particle systems [29–33], diffusions [34–36], and quantum systems [37–41]. For the SDE (1), preliminary results [26] have shown that the auxiliary process modifies not only the driving γ, which is a natural way to increase or decrease the current, but also the potential $V(\theta)$ in a nonlocal and nonlinear way. Here, we complete these results by constructing the auxiliary process for a wider range of parameters and by relating it to the different fluctuation regimes seen at the level of the large deviation functions. We also study fluctuation symmetries for J_T, related to the so-called fluctuation relation for the entropy production [5–7], and we demonstrate an entropic bound for the rate function recently derived in [42] (see also [43]).

The results that we obtain show a rich tradeoff between modifying γ and $V(\theta)$ to reach low or high current fluctuations, yielding many physical insights about how these fluctuations arise in time. This is particularly useful for understanding the low-noise limit of large deviations, studied within the so-called Freidlin-Wentzell theory [13] (see also [44]) or the macroscopic fluctuation theory [45–47] in terms of most probable paths or instantons minimizing a given stochastic action. We show here how to use the deterministic limit of the auxiliary process as an alternative way to recover these instantons. Using this technique, we are able to clarify certain properties of the rate function for the circle diffusion related to a dynamical phase transition.

II. CURRENT LARGE DEVIATIONS

In this section, we briefly explain the large deviation formalism used to describe the probability distribution of J_T in the long-time limit and how the auxiliary process is constructed from spectral elements related to the large deviations of J_T. For background material on large deviations, see [48–50].

A. Large deviation principle

The paths of pure diffusions are nowhere differentiable, as is well known, so the expression of the current shown in (3)

*tsobgnipelerine@gmail.com
†htouchette@sun.ac.za, htouchet@alum.mit.edu

 ©2016 American Physical Society

is only a formal expression that we replace mathematically by the stochastic integral

$$J_T = \frac{1}{T}\int_0^T d\theta_t = \frac{(\theta_T - \theta_0)N_T}{T}, \tag{4}$$

where N_T is the *winding number*, that is, the net number of turns done by θ_t through $\theta = 0$ (or any other angle) after a time T. Alternatively, we can write

$$J_T = \frac{\theta_T - \theta_0}{T} \tag{5}$$

by considering θ_t to be a multivalued angle taking values in $\mathbb{R}$ instead of $[0,2\pi)$. Without loss in generality, we choose $\theta_0 = 0$ as the initial angle.

In the infinite-time or ergodic limit, J_T is known to converge to the average speed $\langle J_T\rangle$, given for the driven periodic diffusion by the expectation

$$\langle J_T\rangle = \langle F(\theta)\rangle \tag{6}$$

of the total force

$$F(\theta) = \gamma - V'(\theta) \tag{7}$$

driving the SDE (1). The exact expression of this expectation, due to Stratonovich, can be found in [1] [see also the formula (25) in [7]]. With this result, we thus have

$$\lim_{T\to\infty} J_T = \langle F\rangle \tag{8}$$

for almost all paths of the diffusion, which means that, although J_T fluctuates around its mean, it converges almost surely to it as $T \to \infty$. For this reason, the mean is also called the *concentration point* of J_T.

We are interested here in the rare fluctuations of J_T around this concentration point. Following the theory of large deviations (see, e.g., [48–50]), the probability of these fluctuations has the general form

$$P(J_T = j) \approx e^{-TI(j)} \tag{9}$$

in the limit $T \to \infty$. The approximation sign means that corrections to the exponential term are sublinear in T in the exponent, which means that the exponential itself is the dominant term of $P(J_T = j)$ at large times. The function $I(j)$ given by the limit

$$I(j) = \lim_{T\to\infty} -\frac{1}{T}\ln P(J_T = j) \tag{10}$$

is called the *rate function* and is so named because it controls the rate at which the probability $P(J_T = j)$ decays to zero for any $j \neq \langle J_T\rangle$ as $T \to \infty$. As a result, we have $I(\langle J_T\rangle) = 0$ and $I(j) > 0$ for any other values of j, showing that the fluctuations of J_T away from its mean are exponentially unlikely at large times.

For the model studied here, $I(j)$ is exactly quadratic and equal to

$$I(j) = \frac{(j-\gamma)^2}{2\sigma^2} \tag{11}$$

when $V_0 = 0$ [8]. For other parameter values, it has a nontrivial shape characterizing non-Gaussian current fluctuations coming from the interplay between the potential $V(\theta)$ and the nonequilibrium drive γ.

B. Large deviation functions

Many methods can be used to obtain the rate function $I(j)$; here we use the Gärtner-Ellis Theorem [48–50], which states that $I(j)$ is given by the Legendre-Fenchel transform of the scaled cumulant generating function (SCGF) of J_T,

$$\lambda(k) = \lim_{T\to\infty}\frac{1}{T}\ln\langle e^{TkJ_T}\rangle, \tag{12}$$

when the latter function exists and is differentiable for $k \in \mathbb{R}$. Thus,

$$I(j) = \sup_{k\in\mathbb{R}}\{kj - \lambda(k)\} \tag{13}$$

under these conditions.

For time-integrated observables of Markov processes such as J_T, $\lambda(k)$ is known to be given by the dominant eigenvalue of a modified linear operator, called the *tilted generator*, which corresponds here to

$$\mathcal{L}_k = F\left(\frac{d}{d\theta} + k\right) + \frac{\sigma^2}{2}\left(\frac{d}{d\theta} + k\right)^2 \tag{14}$$

and which acts on periodic functions of $[0,2\pi)$ (see [28] for the derivation of this operator). As a result, we write

$$\mathcal{L}_k r_k(\theta) = \lambda(k) r_k(\theta), \tag{15}$$

where $\lambda(k)$ is the dominant eigenvalue of $\mathcal{L}_k$ and $r_k(\theta)$ is its corresponding (periodic) eigenfunction.

For $k = 0$, $\mathcal{L}_0 = L$ is simply the generator of the SDE (1) having the trivial eigenfunction $r_0(\theta) = 1$, which is conjugated to the stationary density $\rho^{\text{inv}}(\theta)$ solving the Fokker-Planck equation

$$L^\dagger \rho^{\text{inv}} = 0, \tag{16}$$

where $L^\dagger$ is the adjoint of L. The stationary density $\rho^{\text{inv}}(\theta)$ is unique, since the process is defined on a compact space, and it is given by an explicit formula for all parameter values; see Chap. 11 of [18]. The compactness of the space also implies that the spectrum of $\mathcal{L}_k$ is discrete. It is real in the equilibrium case ($\gamma = 0$) and is composed otherwise of complex-conjugate pairs of eigenvalues, except for the dominant eigenvalue $\lambda(k)$, which is always real.

The non-Hermitian spectral problem (15) has no known solution, except for $k = 0$ and for $V_0 = 0$. However, its general solution can be constructed easily, following [6], by means of a Fourier-Bloch decomposition of the eigenfunction

$$r_k(\theta) = \sum_{n\in\mathbb{Z}} c_n e^{in\theta} \tag{17}$$

and the potential derivative

$$V'(\theta) = \sum_{n\in\mathbb{Z}} v_n e^{in\theta}. \tag{18}$$

Substituting these expansions in (15) yields a recurrence relation for the coefficients c_n, which reduces for the cosine potential (2) to

$$b_n^- c_{n-1} + [a_n - \lambda(k)]c_n + b_n^+ c_{n+1} = 0, \tag{19}$$

where

$$a_n = in(\gamma + \sigma^2 k) - \frac{\sigma^2 n}{2} + k\gamma + \frac{k^2\sigma^2}{2},$$
$$b_n^{\pm} = \frac{V_0}{2}(\pm ik - 1 \mp n). \tag{20}$$

To solve this tridiagonal system, we naturally truncate n to some discrete range $[[-M,M]]$, yielding a system of $2M+1$ linearly independent equations, which are solved numerically to find the coefficients c_n of $r_k(\theta)$, the SCGF $\lambda(k)$, and the rate function $I(j)$ by Legendre-transforming $\lambda(k)$. We present the results of these calculations for various parameters in the next section. In all cases, we have checked that the results converge for M large enough, and we only present the largest M used, which is typically between $M = 5$ and 30 modes depending mostly on the ratio σ/V_0. In general, the smaller σ/V_0 is, the larger M must be chosen [51].

For the rest of the paper, it is useful to note that the large deviation functions $\lambda(k)$ and $I(j)$ can also be obtained in a very different way via optimization problems derived in [27] (see also [10,11,52]). For the SCGF, the optimization to solve is

$$\lambda(k) = \inf_u \{k\langle u\rangle_u - K(u)\}, \tag{21}$$

where

$$K(u) = \frac{1}{2\sigma^2}\int_0^{2\pi} [u(\theta) - F(\theta)]^2 \rho_u^{\text{inv}}(\theta)\, d\theta \tag{22}$$

and

$$\langle u\rangle_u = \int_0^{2\pi} u(\theta)\rho_u^{\text{inv}}(\theta) d\theta \tag{23}$$

is the average current calculated with respect to the stationary density ρ_u^{inv} of a diffusion with total force u, that is, the stationary density solving the Fokker-Planck equation (16) with F replaced by u. By Legendre duality, the rate function is then obtained by solving the constrained optimization

$$I(j) = \inf_{u:\langle u\rangle_u = j} K(u). \tag{24}$$

In both cases, the optimization is over all continuous and periodic functions $u(\theta)$.

Similar optimizations were considered in [9–11] as a way to study the large deviations of the ring model. They are difficult to solve in general, but can be expanded in Fourier-Bloch modes at the level of $u(\theta)$ to give what is essentially the eigenfunction $r_k(\theta)$ constructed above. In some cases, exact solutions can be found, as will be discussed in the next section, in addition to approximate solutions for $u(\theta)$, which yield useful approximations and bounds for $\lambda(k)$ and $I(j)$.

C. Effective fluctuation process

The auxiliary or driven process mentioned in the Introduction is constructed from the dominant eigenfunction $r_k(\theta)$ as the new diffusion $\hat{\theta}_t$ given by the SDE,

$$d\hat{\theta}_t = F_k(\hat{\theta})dt + \sigma\, dW_t, \tag{25}$$

which involves the same noise as θ_t but a modified force

$$F_k(\theta) = F(\theta) + \sigma^2\left(k + \frac{d}{d\theta}\ln r_k(\theta)\right) \tag{26}$$

compared to the force $F(\theta)$ of θ_t [26]. The idea again behind this process is to understand how the original process θ_t reaches a current fluctuation $J_T = j$ after a long time T [26]. In mathematical terms, this means that we must condition θ_t on the event $J_T = j$ and infer from this conditioning a new Markov process that describes the set of "constrained" paths of θ_t such that $J_T = j$ [28].

The auxiliary process is that Markov process. To be more precise, it is the process that is *equivalent to the conditioned process in the long-time limit*, in the same way that the canonical ensemble is equivalent to the microcanonical ensemble in the infinite-volume limit [28]. In fact, equivalence is achieved similarly to equilibrium by relating the constant current j of the conditioned (microcanonical) process to the "temperature" k of the auxiliary (canonical) process according to [26]

$$I'(j) = k \tag{27}$$

or, equivalently,

$$\lambda'(k) = j. \tag{28}$$

From this, it is natural to interpret $\hat{\theta}_t$ as the effective process that "creates" the fluctuation $J_T = j$, just as the canonical ensemble "creates" in the thermodynamic limit a microcanonical ensemble with fixed energy. Naturally, $F_{k=0} = F$ since $\lambda'(0) = \langle J_T\rangle$.

It is worth emphasizing that the constraint $J_T = j$ is not satisfied at all times in the auxiliary process. What we have again is a long-time or ergodic equivalence implying that $J_T \to j$ for this process as $T \to \infty$. As a result, the rare event that is $J_T = j$ for θ_t is transformed into a typical event for $\hat{\theta}_t$, which is useful for simulations [27]. From the point of view of control theory, it can be shown that this change of process minimizes $K(u)$ above, so that the optimal $u(\theta)$ in (21) or (24) is actually $F_k(\theta)$ [27]. This explains why the Fourier-Bloch solution for $u(\theta)$ is equivalent, as mentioned, to the Fourier-Bloch solution for $r_k(\theta)$. The two are related by (26).

III. RESULTS

In this section, we present the results of the Fourier-Bloch solution of the large deviation functions and the auxiliary process. Some of these results are related to the large deviations of the mean entropy production Σ_T [5–7], which is linearly related to the current J_T according to

$$\Sigma_T = \frac{2\gamma}{\sigma^2}J_T - \frac{2}{\sigma^2 T}[V(\theta_T) - V(\theta_0)], \tag{29}$$

while others have appeared in the context of variational approaches to large deviations [9–11]. Consequently, our discussion of the large deviation functions, which are known to some extent, will be brief. Our main goal, as mentioned before, is to explain with the auxiliary process how the different fluctuation regimes inferred from these functions arise physically.

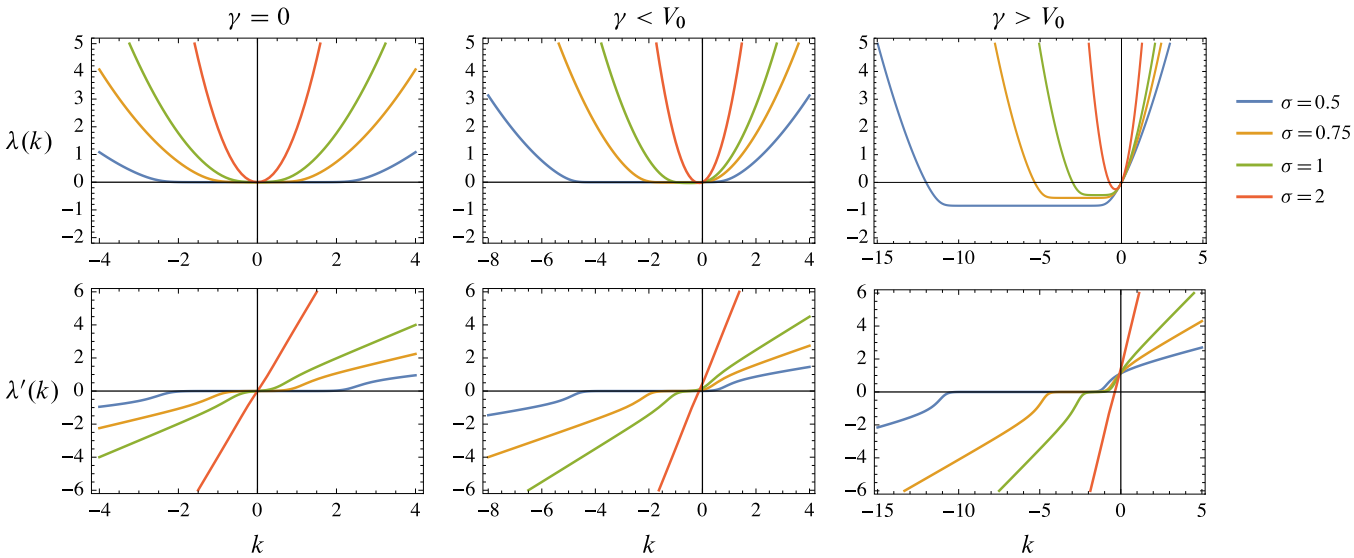

FIG. 1. Top row: SCGF for different values of σ. Bottom row: derivative of the SCGF. Parameters: $V_0 = 1$, $\gamma = 0$ (left column), $\gamma = 0.5$ (middle column), $\gamma = 1.5$ (right column).

To understand these results, it is important to note that the noiseless ($\sigma = 0$) dynamics undergoes a bifurcation between a *fixed-point solution* for $|\gamma| \leqslant V_0$, where $\dot{\theta}_t \to 0$ after some transient time so that $J_T \to 0$, and a *running solution* for $|\gamma| > V_0$, where θ_t rotates in such a way that

$$\lim_{T\to\infty} J_T = \sqrt{\gamma^2 - V_0^2} \tag{30}$$

for $\gamma > V_0$ [53]. This bifurcation is "rounded" by the noise, but it still determines much of the different fluctuation regimes discussed next.

A. Current fluctuations

We show in Fig. 1 the plot of $\lambda(k)$ as a function of k for different values of γ and σ, together with the plot of its derivative for the same parameters. From the results, we can see that the current fluctuations are essentially Gaussian at high noise (i.e., large σ relative to V_0), since $\lambda(k)$ is then a parabola (with linear slope), which implies that the rate function $I(j)$, obtained by the Legendre transform (13), is also a parabola, as seen in Fig. 2. For low noise, $\lambda(k)$ develops instead a flat plateau giving rise, by Legendre transform, to a "kink" in $I(j)$ around $j = 0$, indicating a non-Gaussian crossover between negative and positive fluctuations. Far from $j = 0$, the fluctuations become Gaussian again, as can be seen by the fact that $\lambda'(k)$ is linear away from its plateau.

This picture remains more or less the same when the nonequilibrium drive γ is increased; all that changes is the value of $\lambda'(0)$, which determines the zero of $I(j)$ and thus the mean current, shown in Fig. 3. From this plot, we see that $\langle J_T \rangle$ is essentially zero in the fixed-point regime when σ is small and grows according to (30) in the running regime. For large σ, we find instead $\langle J_T \rangle \approx \gamma$. In each case, the kink of the rate function $I(j)$ remains at $j = 0$, despite the zero of $I(j)$ moving with γ, and becomes more pronounced as $\sigma \to 0$.

This kink was already reported for the entropy production [5–7] and is akin to dynamical phase transitions seen in the activity or current fluctuations of particle models [54–59] and disordered random walks [60]. For the ring model, there is no dynamical phase transition properly speaking because $\lambda(k)$ is not exactly flat in the plateaus: it only grows very slowly from a central minimum, as can be verified by zooming in the plateau. This implies that $I(j)$ has a rounded kink at $j = 0$ with continuous derivative instead of an actual cusp with discontinuous derivative. In general, for $\lambda(k)$ and $I(j)$ to have nonanalytic points, determining either a phase transition in the mean of J_T or a dynamical phase transition in its fluctuations, there needs to be a thermodynamic or scaling limit, such as the noiseless limit studied in Sec. IV [61].

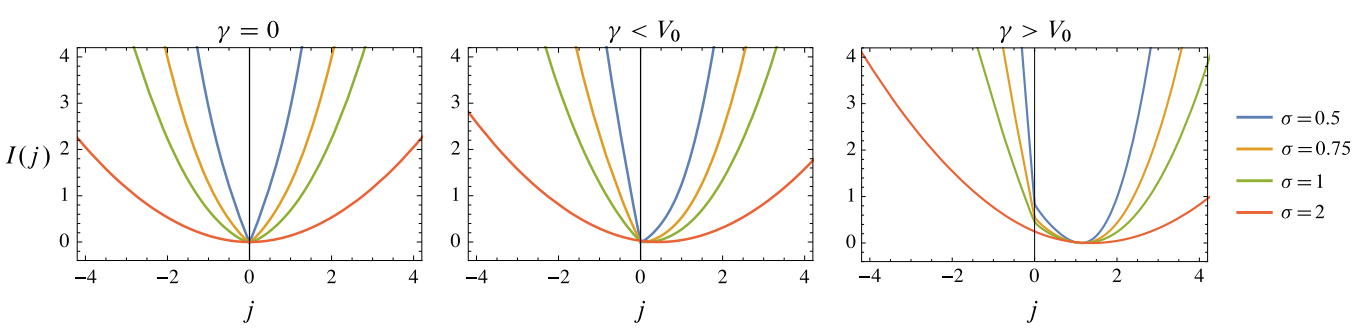

FIG. 2. Rate function for different values of σ. Parameters: $V_0 = 1$, $\gamma = 0$ (left column), $\gamma = 0.5$ (middle column), $\gamma = 1.5$ (right column).

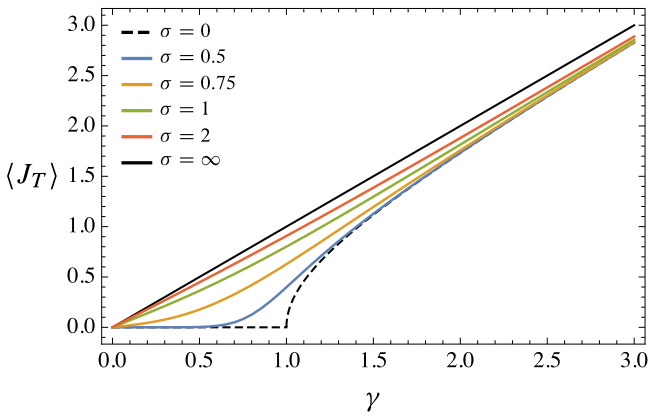

FIG. 3. Mean current as a function of γ for $V_0 = 1$. The mean current is given by $\lambda'(0)$ or, equivalently, by the zero of $I(j)$.

Another crossover in the fluctuations can be seen at the level of $\lambda''(0)$, which determines the asymptotic variance of J_T according to

$$\lambda''(0) = \lim_{T\to\infty} T \operatorname{var}(J_T). \tag{31}$$

The plot of this quantity in Fig. 4 shows that the current fluctuations around the mean are enhanced near the bifurcation point $\gamma = V_0$, especially at low noise. This is commonly observed in noisy dynamics undergoing bifurcations or phase transitions. A similar crossover, referred to as a "giant acceleration" or "giant response," is observed for the long-time variance of θ_t, which determines the diffusion coefficient [1–3].

B. Auxiliary process

The two mean features of the current fluctuations just discussed, namely the rounded kink at $j = 0$ and the large Gaussian fluctuations away from that kink, can be understood in a clear and physical way by analyzing the auxiliary process. To that end, we show in Fig. 5 the modified force $F_k(\theta)$ of this process, given by (26), for the same values of γ as in Fig. 1. We also show $F_k(\theta)$ in each plot for different values of k in the ranges used in Fig. 1.

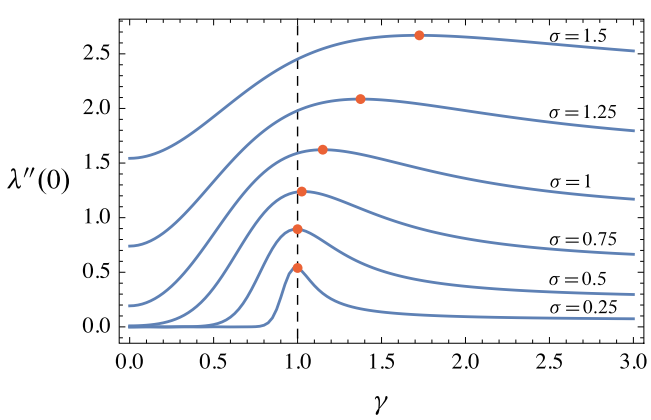

FIG. 4. Asymptotic current variance as a function of γ for $V_0 = 1$ and different values of σ. The dots show the maximum of each curve.

From the left plot of Fig. 5, corresponding to $\gamma = 0$, we clearly see that the effective process associated with large values of $|k|$ (blue and green curves), which encode the large current fluctuations, is to a good approximation a simple diffusion with constant drift given by $F_k(\theta) = \sigma^2 k$. Using this in the variational representation (21), we then find

$$\lambda(k) \approx \frac{\sigma^2 k^2}{2} \tag{32}$$

to leading order in k, which yields from either (13) or (24),

$$I(j) \approx \frac{j^2}{2\sigma^2}. \tag{33}$$

For large fluctuations, the diffusion therefore acts as if there were no potential: the natural drive γ is simply modified to create a larger or smaller current. This is the most efficient way of creating large current values, and it leads, according to (24), to Gaussian fluctuations, as in the case $V_0 = 0$.

For the fluctuations close to $j = 0$, corresponding to low values of k (orange curves), the effective force is not so trivial. Instead of being globally shifted upward or downward, it is modified locally away from the fixed point $\theta = \pi$ in such a way as to bring the unstable fixed point, corresponding to the other node of $F_k(\theta)$, closer to π. This has the effect of lowering the potential barrier associated with F_k on the left or right of the fixed point, depending on the sign of k, thereby creating a small positive or negative current. This is an optimal strategy for creating a current according to (24), as $(u - F)^2$ is minimized around the fixed point where θ_t spends most of its time and where $\rho_u^{\mathrm{inv}}(\theta)$ is therefore maximum. The fluctuations in this case are non-Gaussian because of the nonconstant change from F to F_k.

This dichotomous picture between large fluctuations created by an effective constant drive, on the one hand, and small fluctuations created by lowering the potential barrier, on the other, is consistent physically with what we see for the mean current and also explains the results obtained for $\gamma \neq 0$. In this case, the auxiliary force is shifted to $F_k(\theta) = \gamma + \sigma^2 k$ for large $|k|$, which yields the Gaussian approximation

$$I(j) \approx \frac{(j-\gamma)^2}{2\sigma^2} \tag{34}$$

for the large current fluctuations. For $\gamma > 0$, the range of k where $F_k(\theta)$ has a fixed point, leading to non-Gaussian fluctuations close to $j = 0$, is also extended and shifted relative to $F(\theta)$; see Fig. 5. This fixed-point region is studied in more detail in Sec. IV to obtain $I(j)$ as $\sigma \to 0$.

C. Fluctuation relation and upper bounds

The SCGF and rate function of the current are constrained by the general symmetry of the entropy production,

$$\frac{P(\Sigma_T = s)}{P(\Sigma_T = -s)} = e^{Ts}, \tag{35}$$

which implies, by applying the change of variables (29) and by neglecting the potential boundary terms [62],

$$I(-j) = I(j) + cj \tag{36}$$

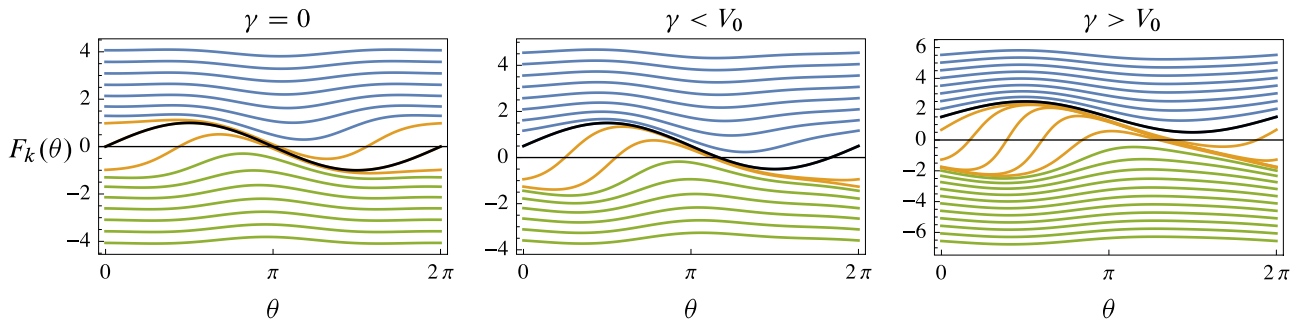

FIG. 5. Effective force $F_k(\theta)$ of the auxiliary process for the same values of γ as in Fig. 1. The curves in each plot show F_k for different values of k taken, in spacing of 0.5, in the ranges of $\lambda(k)$ used in Fig. 1. Black curve: $F_0 = F$; blue curves: F_k associated with positive current fluctuations; green curves: F_k associated with negative current fluctuations; orange curves: F_k with stable fixed points (nodes) associated with near-zero current fluctuations. Other parameters: $V_0 = 1$, $\sigma = 1$.

or equivalently

$$\lambda(k) = \lambda(-k - c), \tag{37}$$

where $c = 2\gamma/\sigma^2$. These symmetries for the large deviation functions are collectively referred to as *fluctuation relations* [63–66] (see [67] for a review) and are connected for the entropy production to a general symmetry of its tilted generator; see Sec. 5 of [66]. For the current, this operator symmetry, which takes the form

$$\mathcal{L}_k^\dagger = \mathcal{L}_{-k-c}, \tag{38}$$

is not *a priori* satisfied, since J_T is only proportional to Σ_T in the limit $T \to \infty$ because of the potential boundary terms in (29). For $V_0 = 0$, however, J_T is exactly proportional to Σ_T for all T, so the operator symmetry (38) holds, as can be verified from the expression (14) of $\mathcal{L}_k$. In this case, the symmetry (37) thus holds, not just for the dominant eigenvalue in fact but for the whole spectrum.

Two upper bounds constraining $\lambda(k)$ and $I(j)$ can also be derived. The first follows by noting, as before, that the auxiliary force is asymptotically given by $F_k(\theta) = \gamma + \sigma^2 k$ as $k \to \pm\infty$. Inserting this in the variational principle (24) yields

$$I_{\text{aux}}(j) = \frac{(j-\gamma)^2}{2\sigma^2} + \frac{V_0^2}{4\sigma^2}, \tag{39}$$

and since this is not the true minimizer of (21) in general, we must have

$$I(j) \leqslant I_{\text{aux}}(j). \tag{40}$$

The second bound follows from a result recently derived for jump processes in [42] (see also [43]), which here takes the form

$$I(j) \leqslant I_{\text{ent}}(j) = \frac{(j-j^*)^2}{4j^{*2}}\Sigma^*, \tag{41}$$

where $\Sigma^* = 2\gamma j^*/\sigma^2$ is the mean entropy production associated with the mean current $j^* = \lambda'(0)$.

These two bounds are quadratic in j but limit the rate function in different ways, as can be seen in Fig. 6. The entropic bound (41) is tight at the mean current j^* as well as at $-j^*$, since it satisfies the fluctuation relation (36), but departs from the true $I(j)$ in the tails. By contrast, the bound (40) obtained from the auxiliary process approximation is tight in the tails but not around the mean by construction. It also gives a nontrivial bound for $\gamma = 0$. The two bounds are identical and in fact equal to $I(j)$ when $V_0 = 0$, since $I(j)$ is again exactly quadratic with $j^* = \gamma$.

IV. LOW-NOISE LIMIT

The exact result (11) obtained for $V_0 = 0$ and the numerical results shown in Fig. 2 for $V_0 \neq 0$ suggest the following scaling of the rate function:

$$I(j) \sim \frac{\tilde{I}(j)}{\sigma^2} \tag{42}$$

as $\sigma \to 0$. This scaling is also expected from the Freidlin-Wentzell-Graham (FWG) theory of large deviations in the low-noise limit [13,44] and implies the following large deviation principle for the current distribution:

$$P(J_T = j) \approx e^{-T\tilde{I}(j)/\sigma^2} \tag{43}$$

in the limit of large T and small σ.

Our goal in this section is to obtain the rescaled rate function

$$\tilde{I}(j) = \lim_{\sigma\to 0} \sigma^2 I(j) \tag{44}$$

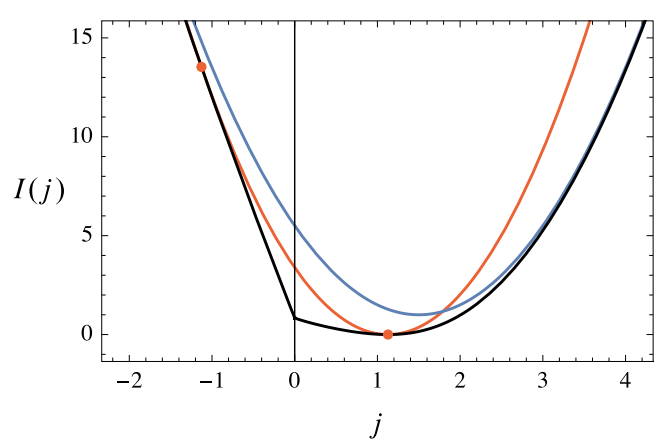

FIG. 6. Auxiliary upper bound (blue curve) and entropic upper bound (red curve) on the rate function $I(j)$ (black curve). The two dots mark the points (j^* and $-j^*$) where the entropic bound touches $I(j)$. Parameters: $V_0 = 1$, $\gamma = 1.5$, $\sigma = 0.5$.

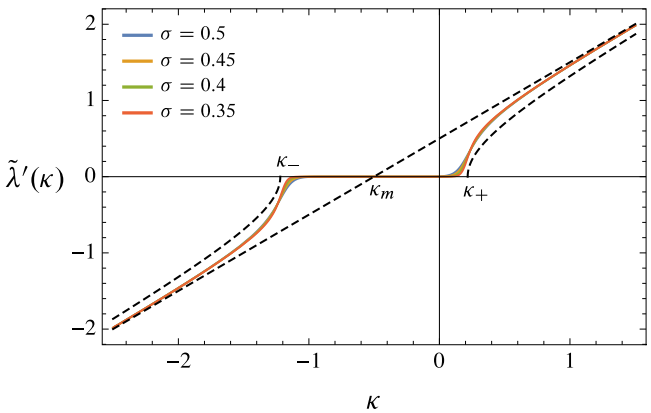

FIG. 7. Derivative of the rescaled SCGF. Parameters: $V_0 = 1$, $\gamma = 0.5$. Dashed lines: linear and hyperbolic approximations.

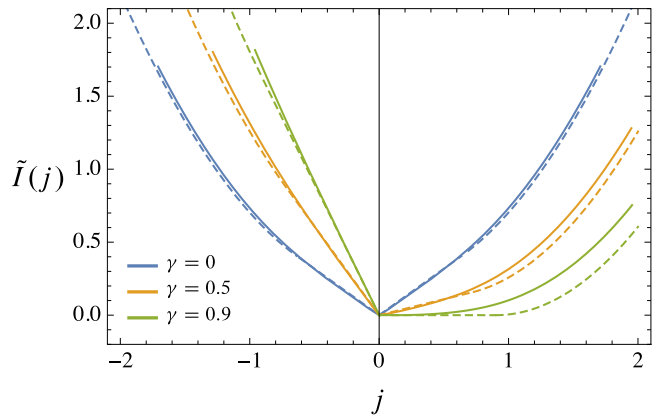

FIG. 8. Full lines: rescaled rate function obtained with $\sigma = 0.35$. Dashed lines: piecewise-parabolic approximation. Other parameter: $V_0 = 1$.

characterizing the current fluctuations in this limit. Unfortunately, it is not possible to obtain this function analytically or numerically for $\sigma = 0$: finding the zero-noise limit of the spectrum of $\mathcal{L}_k$, which is similar to the semiclassical limit of Schrödinger-type operators (see [68]), is a difficult problem, even more so for non-Hermitian operators, and the numerical diagonalization method that we use becomes ill-conditioned for low σ relative to V_0 [51]. However, we can combine the numerical results that we have with analytical results derived from a random-walk approximation of the diffusion [6,7,66] to obtain a good approximation of the current rate function in the low-noise limit. This is done next.

A. Rescaled large deviations

The rescaled rate function is obtained by rescaling the Legendre transform (13) as

$$\tilde{I}(j) = \sup_{\kappa}\{\kappa j - \tilde{\lambda}(\kappa)\}, \tag{45}$$

where

$$\tilde{\lambda}(\kappa) = \lim_{\sigma\to 0} \sigma^2 \lambda\left(\frac{\kappa}{\sigma^2}\right) \tag{46}$$

is the corresponding rescaled SCGF. The result of this scaling is shown for $\tilde{\lambda}'(\kappa)$ in Fig. 7 and suggests the following properties of $\tilde{\lambda}(\kappa)$ whenever $\gamma < V_0$:

(i) Central plateau: $\tilde{\lambda}(\kappa) = 0$ for $\kappa \in [\kappa_-,\kappa_+]$.

(ii) Parabolic branches: Far away from the plateau,

$$\tilde{\lambda}'(\kappa) \sim \kappa - \kappa_m, \tag{47}$$

where $\kappa_m = (\kappa_+ + \kappa_-)/2$, implying

$$\tilde{\lambda}(\kappa) \sim \frac{(\kappa - \kappa_m)^2}{2} \tag{48}$$

for $\kappa \gg \kappa_+$ and $\kappa \ll \kappa_-$.

(iii) Crossover regions: $\tilde{\lambda}'(\kappa)$ approaches κ_+ and κ_- continuously, which implies that $\tilde{\lambda}(\kappa)$ is continuous with continuous derivatives at these points.

Property (i) is consistent with the random walk [6] and FWG approximations [7] of the rate function close to $j = 0$, which, when transposed to $\tilde{I}(j)$, predict that $\tilde{I}(j)$ has a genuine cusp at $j = 0$ with left and right derivatives given by

$$\tilde{I}(0^-) = -\frac{\Delta U_-}{\pi} = \frac{1}{\pi}\int_{\theta_s+2\pi}^{\theta_u} F(\theta)d\theta \tag{49}$$

and

$$\tilde{I}(0^+) = \frac{\Delta U_+}{\pi} = -\frac{1}{\pi}\int_{\theta_s}^{\theta_u} F(\theta)d\theta, \tag{50}$$

respectively. Here, θ_s and θ_u are the stable and unstable fixed points of $F(\theta)$, respectively, so that ΔU_- and ΔU_+ are interpreted as the potential barriers created by $F(\theta)$ on the left and the right of θ_s, respectively. By Legendre transform, $\tilde{\lambda}(\kappa)$ must then have a genuine plateau for $\kappa \in [\kappa_-,\kappa_+]$ with κ_- and κ_+ equal to the derivatives above. This is confirmed by our numerical results, which show that the range $[k_-,k_+]$ where the nonscaled $\lambda(k)$ appears to have a flat plateau grows with σ according to

$$\sigma^2 k_\pm = \kappa_\pm + O(\sigma^2). \tag{51}$$

Rescaling $\lambda(k)$ using (46) then implies that $\tilde{\lambda}(\kappa)$ has a fixed plateau over $[\kappa_-,\kappa_+]$ that does not scale with σ. Property (ii) follows from the same rescaling by noting that $\lambda(k) \sim \sigma^2 k^2/2$ for large $|k|$.

These results for $\tilde{\lambda}(\kappa)$ imply, as already mentioned, that $\tilde{I}(j)$ has a cusp at $j = 0$ and parabolic branches. This is verified in Fig. 8, which shows $\tilde{I}(j)$ as obtained by rescaling $I(j)$ for $\sigma = 0.35$, the lowest σ that is stable numerically. The cusp is clearly visible and has slopes matching the expected values κ_- and κ_+. Moreover, it can be verified from (49) and (50) that

$$\kappa_+ + \kappa_- = -2\gamma, \tag{52}$$

in agreement with the fluctuation relation (36) rescaled to $\tilde{I}(j)$. When $\gamma = 0$, for example,

$$\kappa_+ = -\kappa_- = \frac{2}{\pi}, \tag{53}$$

whereas for $\gamma = V_0$, $\kappa_+ = 0$ and $\kappa_- = -2\gamma$. In all cases, $\kappa_m = -\gamma$.

In the crossover regions close to κ_- and κ_+, we are not able to determine the exact behavior of $\tilde{\lambda}(\kappa)$. As a simple

approximation, we can write

$$\tilde{\lambda}'(\kappa) \approx \begin{cases} \kappa - \kappa_m, & \kappa \notin [\kappa_-,\kappa_+], \\ 0, & \kappa \in [\kappa_-,\kappa_+] \end{cases} \tag{54}$$

leading to

$$\tilde{\lambda}(\kappa) \approx \begin{cases} \frac{(\kappa-\kappa_m)^2}{2} - \frac{\nu_+^2}{2}, & \kappa > \kappa_+, \\ 0, & \kappa \in [\kappa_-,\kappa_+], \\ \frac{(\kappa-\kappa_m)^2}{2} - \frac{\nu_-^2}{2}, & \kappa < \kappa_-, \end{cases} \tag{55}$$

where

$$\nu_\pm = \kappa_\pm - \kappa_m = \frac{\kappa_\pm - \kappa_\mp}{2}. \tag{56}$$

The rate function obtained from this piecewise-parabolic approximation shows a fairly good agreement with $\tilde{I}(j)$ for $\gamma \approx 0$, as shown in Fig. 8. A better approximation is obtained for $\gamma \lesssim V_0$ by replacing the derivative jumps in (54) by hyperbolic branches, similar to the deterministic case (see Fig. 3), starting at κ_- and κ_+. Both approximations recover the cusp of $\tilde{I}(j)$ at $j = 0$ and also satisfy the fluctuation relation.

These results apply for $\gamma < V_0$, which corresponds to the fixed-point regime where $j^* = 0$ in the low-noise limit. For $\gamma \geqslant V_0$, the values of κ_- and κ_+ are no longer given by (49) and (50), since there are no fixed points in the running regime. The random-walk approximation is also not applicable anymore, but our numerical results still suggest that $\tilde{\lambda}'(\kappa)$ has the generic form shown in Fig. 7 with κ_- and κ_+ satisfying (52) so that $\kappa_m = -\gamma$. The rate function, therefore, also has in this case a cusp at $j = 0$ with left and right slopes given by κ_- and κ_+, respectively and is a parabola for large and small current values, which does not depend on V_0 as before. The potential, as in the case $\gamma < V_0$, only determines the region of $I(j)$ near the cusp.

B. Auxiliary process and instantons

We conclude our study of the driven periodic diffusion by comparing the low-noise instanton solution obtained from the FWG theory and the force of the auxiliary process rescaled with $\kappa = \sigma^2 k$. We do not repeat the FWG calculation; see Sec. 3.4 of [7]. The basic idea is that $\tilde{I}(j)$ is determined by a deterministic trajectory, called the most probable path or instanton, which minimizes the path action

$$\mathcal{I}_T[\theta] = \frac{1}{2T}\int_0^T [\dot{\theta}_t - F(\theta_t)]^2\, dt \tag{57}$$

subject to the constraint $J_T = j$. Thus

$$\tilde{I}(j) = \lim_{T\to\infty} \min_{\theta_t : J_T = j} \mathcal{I}_T[\theta] = \mathcal{I}_\infty[\theta^*], \tag{58}$$

where $\{\theta_t^*\}_{t=0}^T$ is the instanton solving the constrained optimization problem.

We plot in Fig. 9 the time derivative of θ_t^* as a function of θ_t^* (modulo 2π) to obtain the dynamics of the instanton as

$$\dot{\theta}_t^* = G_j(\theta_t^*) \tag{59}$$

for different values of the constraint $J_T = j$, and we compare the effective force $G_j(\theta)$ [69] thus obtained for the instanton

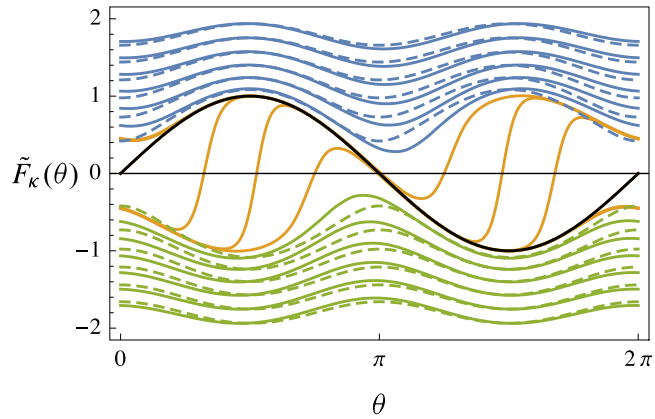

FIG. 9. Full curves: effective force $\tilde{F}_\kappa(\theta)$ of the auxiliary process after rescaling k (see Fig. 5 for the color code). Dashed curves: instanton force $G_j(\theta)$ obtained from the FWG calculation. Parameters: $\gamma = 0$, $V_0 = 1$, $\sigma = 0.4$.

with the effective force of the auxiliary process rescaled as

$$\tilde{F}_\kappa(\theta) = \lim_{\sigma\to 0} F_{k=\kappa/\sigma^2}(\theta) \tag{60}$$

to follow the rescaling (46) of the SCGF. The results for G_j and $\tilde{F}_\kappa$ are in good agreement, given that we can only calculate the latter numerically for σ no smaller than 0.4, and they are consistent with the idea that the instanton dynamics corresponds to the $\sigma \to 0$ limit of the auxiliary process [28]. In that limit, the SDE (25) does indeed converge to the following differential equation:

$$\dot{\theta}_t = \tilde{F}_\kappa(\theta_t), \tag{61}$$

which must coincide with (59), after matching κ to the current fluctuation j via $\tilde{\lambda}'(\kappa) = j$, in order for the optimization problem (24) to be consistent with the FWG optimization (58). The former optimization is solved by the auxiliary dynamics, while the latter is solved by the instanton dynamics. Since both give the same rate function, they must therefore describe the same deterministic dynamics.

With this correspondence, we can understand the dynamical phase transition associated with the cusp of $\tilde{I}(j)$ by noting that, although the effective force $\tilde{F}_\kappa$ of the auxiliary process is continuous in κ, it does not create any current for $\kappa \in [\kappa_-,\kappa_+]$, in agreement with $\tilde{\lambda}'(\kappa) = 0$, since it has a stable fixed point for these values of κ (orange lines in Fig. 9) that prevents rotation as $\sigma \to 0$. Only when $\kappa < \kappa_-$ or $\kappa > \kappa_+$ does the fixed point disappear and the dynamics become free to rotate (without noise) to create a negative or positive current (blue and green lines in Fig. 9), determined in the auxiliary dynamics by $\tilde{\lambda}'(\kappa) = j$. The cusp in $\tilde{I}(j)$ appears, therefore, as a result of a "switching" between two solution or dynamics, as is common in first-order or discontinuous phase transitions [70–72]. At the switching point, there is an infinite number of dynamics or solutions determined by $\kappa \in [\kappa_-,\kappa_+]$ that produce no current. This was noticed in [6] and is seen for a different random-walk model [60]. Some features of the dynamical phase transition reported here also arise in the one-dimensional periodic WASEP model [59].

V. CONCLUSION

In this paper, we have studied the current fluctuations of a periodic driven diffusion, often used as a simple model of nonequilibrium systems. Complementing previous studies on this model, we have obtained the large deviation functions of the current, describing its fluctuations in the long-time limit, and have also determined the auxiliary process that explains how these fluctuations are created by an effective noise-induced force. As demonstrated, this auxiliary process is useful for understanding the different fluctuation regimes arising in this model, for deriving bounds on large deviation functions, as well as for deriving the low-noise behavior of the model. Our results, for the latter point, show that the FWG theory of instantons can be obtained by taking the zero-noise limit of the auxiliary dynamics. This is potentially useful for deriving low-noise large deviations of other models, including many-particle models studied within the macroscopic fluctuation theory using the same concepts of most probable paths, instantons, and stochastic action.

For future work, it would be interesting to see whether the numerical results obtained here for the low-noise limit can be obtained analytically from the optimization problems (21) or (24). The existence of a cusp in the rate function is guaranteed by the random-walk approximation of the model, but the precise shape of the rate function around the cusp is yet to be determined analytically. Another interesting problem is to see whether the entropic bound has any interpretation in terms of the auxiliary process. Any process that is not the auxiliary process yields, using the optimization problem (24), an upper bound on the rate function, so it is natural to look again at this problem to understand large deviation bounds.

ACKNOWLEDGMENTS

We thank Krzysztof Gawedzki for sharing his low-noise approximation of the current rate function, as well as Rosemary J. Harris and Carlos Pérez-Espigares for useful comments on this paper. P.T.N. is supported by a DAAD Scholarship. H.T. is supported by the National Research Foundation of South Africa (Grants No. 90322 and No. 96199) and Stellenbosch University (Project Funding for New Appointee).

[1] P. Reimann, C. Van den Broeck, H. Linke, P. Hänggi, J. M. Rubi, and A. Pérez-Madrid, Giant Acceleration of Free Diffusion by Use of Tilted Periodic Potentials, Phys. Rev. Lett. **87**, 010602 (2001).

[2] P. Reimann, C. Van den Broeck, H. Linke, P. Hänggi, J. M. Rubi, and A. Pérez-Madrid, Diffusion in tilted periodic potentials: Enhancement, universality, and scaling, Phys. Rev. E **65**, 031104 (2002).

[3] V. Blickle, T. Speck, C. Lutz, U. Seifert, and C. Bechinger, Einstein Relation Generalized to Nonequilibrium, Phys. Rev. Lett. **98**, 210601 (2007).

[4] U. Seifert and T. Speck, Fluctuation-dissipation theorem in nonequilibrium steady states, Europhys. Lett. **89**, 10007 (2010).

[5] T. Speck, V. Blickle, C. Bechinger, and U. Seifert, Distribution of entropy production for a colloidal particle in a nonequilibrium steady state, Europhys. Lett. **79**, 30002 (2007).

[6] J. Mehl, T. Speck, and U. Seifert, Large deviation function for entropy production in driven one-dimensional systems, Phys. Rev. E **78**, 011123 (2008).

[7] T. Speck, A. Engel, and U. Seifert, The large deviation function for entropy production: The optimal trajectory and the role of fluctuations, J. Stat. Mech. (2012) P12001.

[8] C. Maes, K. Netočný, and B. Wynants, Steady state statistics of driven diffusions, Physica A **387**, 2675 (2008).

[9] F. J. Alexander and G. L. Eyink, Rayleigh-Ritz Calculation of Effective Potential Far from Equilibrium, Phys. Rev. Lett. **78**, 1 (1997).

[10] T. Nemoto and S.-I. Sasa, Variational formula for experimental determination of high-order correlations of current fluctuations in driven systems, Phys. Rev. E **83**, 030105 (2011).

[11] T. Nemoto and S.-I. Sasa, Thermodynamic formula for the cumulant generating function of time-averaged current, Phys. Rev. E **84**, 061113 (2011).

[12] K. Saito and A. Dhar, Waiting for rare entropic fluctuations, Europhys. Lett. **114**, 50004 (2016).

[13] M. I. Freidlin and A. D. Wentzell, *Random Perturbations of Dynamical Systems*, Grundlehren der Mathematischen Wissenschaften Vol. 260 (Springer, New York, 1984).

[14] R. Graham, Fluctuations in the steady state, in *25 Years of Non-Equilibrium Statistical Mechanics*, edited by J. J. Brey, J. Marro, J. M. Rubí, and M. San Miguel (Springer, New York, 1995), pp. 125–134.

[15] A. Faggionato and D. Gabrielli, A representation formula for large deviations rate functionals of invariant measures on the one dimensional torus, Ann. Inst. H. Poincaré Probab. Statist. **48**, 212 (2012).

[16] R. L. Kautz, Thermally induced escape: The principle of minimum available noise energy, Phys. Rev. A **38**, 2066 (1988).

[17] R. L. Kautz, Noise, chaos, and the Josephson voltage standard, Rep. Prog. Phys. **59**, 935 (1996).

[18] H. Risken, *The Fokker-Planck Equation: Methods of Solution and Applications*, 3rd ed. (Springer, Berlin, 1996).

[19] P. Reimann, Brownian motors: Noisy transport far from equilibrium, Phys. Rep. **361**, 57 (2002).

[20] J. R. Gomez-Solano, A. Petrosyan, S. Ciliberto, R. Chetrite, and K. Gawedzki, Experimental Verification of a Modified Fluctuation-Dissipation Relation for a Micron-Sized Particle in a Nonequilibrium Steady State, Phys. Rev. Lett. **103**, 040601 (2009).

[21] S. Ciliberto, S. Joubaud, and A. Petrosyan, Fluctuations in out-of-equilibrium systems: From theory to experiment, J. Stat. Mech. (2010) P12003.

[22] J. R. Gomez-Solano, A. Petrosyan, S. Ciliberto, and C. Maes, Fluctuations and response in a non-equilibrium micron-sized system, J. Stat. Mech. (2011) P01008.

[23] R. M. L. Evans, Rules for Transition Rates in Nonequilibrium Steady States, Phys. Rev. Lett. **92**, 150601 (2004).

[24] R. M. L. Evans, Detailed balance has a counterpart in nonequilibrium steady states, J. Phys. A **38**, 293 (2005).

[25] R. L. Jack and P. Sollich, Large deviations and ensembles of trajectories in stochastic models, Prog. Theor. Phys. Suppl. **184**, 304 (2010).
[26] R. Chetrite and H. Touchette, Nonequilibrium Microcanonical and Canonical Ensembles and Their Equivalence, Phys. Rev. Lett. **111**, 120601 (2013).
[27] R. Chetrite and H. Touchette, Variational and optimal control representations of conditioned and driven processes, J. Stat. Mech. (2015) P12001.
[28] R. Chetrite and H. Touchette, Nonequilibrium Markov processes conditioned on large deviations, Ann. Inst. Poincaré A **16**, 2005 (2015).
[29] V. Popkov, G. M. Schütz, and D. Simon, ASEP on a ring conditioned on enhanced flux, J. Stat. Mech. (2010) P10007.
[30] V. Popkov and G. Schütz, Transition probabilities and dynamic structure function in the ASEP conditioned on strong flux, J. Stat. Phys. **142**, 627 (2011).
[31] R. J. Harris, V. Popkov, and G. M. Schütz, Dynamics of instantaneous condensation in the ZRP conditioned on an atypical current, Entropy **15**, 5065 (2013).
[32] R. L. Jack and P. Sollich, Large deviations of the dynamical activity in the East model: Analysing structure in biased trajectories, J. Phys. A **47**, 015003 (2014).
[33] O. Hirschberg, D. Mukamel, and G. M. Schütz, Density profiles, dynamics, and condensation in the ZRP conditioned on an atypical current, J. Stat. Mech. (2015) P11023.
[34] A. Simha, R. M. L. Evans, and A. Baule, Properties of a nonequilibrium heat bath, Phys. Rev. E **77**, 031117 (2008).
[35] M. Knežević and R. M. L. Evans, Numerical comparison of a constrained path ensemble and a driven quasisteady state, Phys. Rev. E **89**, 012132 (2014).
[36] F. Angeletti and H. Touchette, Diffusions conditioned on occupation measures, J. Math. Phys. **53**, 023303 (2016).
[37] J. P. Garrahan and I. Lesanovsky, Thermodynamics of Quantum Jump Trajectories, Phys. Rev. Lett. **104**, 160601 (2010).
[38] J. P. Garrahan, A. D. Armour, and I. Lesanovsky, Quantum trajectory phase transitions in the micromaser, Phys. Rev. E **84**, 021115 (2011).
[39] C. Ates, B. Olmos, J. P. Garrahan, and I. Lesanovsky, Dynamical phases and intermittency of the dissipative quantum Ising model, Phys. Rev. A **85**, 043620 (2012).
[40] S. Genway, J. P. Garrahan, I. Lesanovsky, and A. D. Armour, Phase transitions in trajectories of a superconducting single-electron transistor coupled to a resonator, Phys. Rev. E **85**, 051122 (2012).
[41] J. M. Hickey, S. Genway, I. Lesanovsky, and J. P. Garrahan, Thermodynamics of quadrature trajectories in open quantum systems, Phys. Rev. A **86**, 063824 (2012).
[42] T. R. Gingrich, J. M. Horowitz, N. Perunov, and J. L. England, Dissipation Bounds All Steady-State Current Fluctuations, Phys. Rev. Lett. **116**, 120601 (2016).
[43] P. Pietzonka, A. C. Barato, and U. Seifert, Universal bounds on current fluctuations, Phys. Rev. E **93**, 052145 (2016).
[44] R. Graham, Macroscopic potentials, bifurcations and noise in dissipative systems, in *Noise in Nonlinear Dynamical Systems*, edited by F. Moss and P. V. E. McClintock (Cambridge University Press, Cambridge, 1989), Vol. 1, pp. 225–278.
[45] L. Bertini, A. De Sole, D. Gabrielli, G. Jona-Lasinio, and C. Landim, Macroscopic fluctuation theory for stationary non-equilibrium states, J. Stat. Phys. **107**, 635 (2002).
[46] L. Bertini, A. De Sole, D. Gabrielli, G. Jona-Lasinio, and C. Landim, Non equilibrium current fluctuations in stochastic lattice gases, J. Stat. Phys. **123**, 237 (2006).
[47] L. Bertini, A. De Sole, D. Gabrielli, G. Jona-Lasinio, and C. Landim, Stochastic interacting particle systems out of equilibrium, J. Stat. Mech. (2007) P07014.
[48] A. Dembo and O. Zeitouni, *Large Deviations Techniques and Applications*, 2nd ed. (Springer, New York, 1998).
[49] F. den Hollander, *Large Deviations*, Fields Institute Monograph (AMS, Providence, 2000).
[50] H. Touchette, The large deviation approach to statistical mechanics, Phys. Rep. **478**, 1 (2009).
[51] In practice, we are able to use MATHEMATICA (version 10) to study noise intensities as small as $\sigma = 0.35$ for $V_0 = 1$, $\gamma \approx V_0$, and k in the relevant range. For smaller values of σ, the linear system to solve becomes unstable.
[52] R. L. Jack and P. Sollich, Effective interactions and large deviations in stochastic processes, Eur. Phys. J. Spec. Top. **224**, 2351 (2015).
[53] S. H. Strogatz, *Nonlinear Dynamics and Chaos* (Addison-Wesley, Reading, MA, 1994).
[54] J. P. Garrahan, R. L. Jack, V. Lecomte, E. Pitard, K. van Duijvendijk, and F. van Wijland, Dynamical First-Order Phase Transition in Kinetically Constrained Models of Glasses, Phys. Rev. Lett. **98**, 195702 (2007).
[55] J. P. Garrahan, R. L. Jack, V. Lecomte, E. Pitard, K. van Duijvendijk, and F. van Wijland, First-order dynamical phase transition in models of glasses: An approach based on ensembles of histories, J. Phys. A **42**, 075007 (2009).
[56] L. O. Hedges, R. L. Jack, J. P. Garrahan, and D. Chandler, Dynamic order-disorder in atomistic models of structural glass formers, Science **323**, 1309 (2009).
[57] J. Hooyberghs and C. Vanderzande, Thermodynamics of histories for the one-dimensional contact process, J. Stat. Mech. (2010) P02017.
[58] A. Dickson, S. M. A. Tabei, and A. R. Dinner, Entrainment of a driven oscillator as a dynamical phase transition, Phys. Rev. E **84**, 061134 (2011).
[59] C. P. Espigares, P. L. Garrido, and P. I. Hurtado, Dynamical phase transition for current statistics in a simple driven diffusive system, Phys. Rev. E **87**, 032115 (2013).
[60] T. R. Gingrich, S. Vaikuntanathan, and P. L. Geissler, Heterogeneity-induced large deviations in activity and (in some cases) entropy production, Phys. Rev. E **90**, 042123 (2014).
[61] It is widely believed, though not proved rigorously, that large deviation functions of time-additive observables are always analytic in the long-time limit for Markov processes with compact state space.
[62] The potential boundary terms can be neglected here because they are bounded. For Markov processes with unbounded state space, such as diffusions in $\mathbb{R}^d$, they have to be included in the large deviation analysis as they can scale with T.
[63] G. Gallavotti and E. G. D. Cohen, Dynamical ensembles in stationary states, J. Stat. Phys. **80**, 931 (1995).
[64] G. Gallavotti and E. G. D. Cohen, Dynamical Ensembles in Nonequilibrium Statistical Mechanics, Phys. Rev. Lett. **74**, 2694 (1995).

[65] J. Kurchan, Fluctuation theorem for stochastic dynamics, J. Phys. A **31**, 3719 (1998).

[66] J. L. Lebowitz and H. Spohn, A Gallavotti-Cohen-type symmetry in the large deviation functional for stochastic dynamics, J. Stat. Phys. **95**, 333 (1999).

[67] R. J. Harris and G. M. Schütz, Fluctuation theorems for stochastic dynamics, J. Stat. Mech. (2007) P07020.

[68] B. Simon, Semiclassical analysis of low lying eigenvalues I. Non-degenerate minima: Asymptotic expansions, Ann. Inst. Henri Poincare: Phys. Th. **38**, 295 (1983).

[69] The effective potential mentioned in [7] is not what we call the effective force G_j for the instanton or the effective force F_k for the auxiliary dynamics.

[70] G. Bunin, Y. Kafri, and D. Podolsky, Cusp singularities in boundary-driven diffusive systems, J. Stat. Phys. **152**, 112 (2013).

[71] Y. Baek and Y. Kafri, Singularities in large deviation functions, J. Stat. Mech. (2015) P08026.

[72] L. Bertini, A. De Sole, D. Gabrielli, G. Jona-Lasinio, and C. Landim, Lagrangian phase transitions in nonequilibrium thermodynamic systems, J. Stat. Mech. (2010) L11001.